Available online at www.sciencedirect.com
ScienceDirect
NDT&E International 39 (2006) 652–660
NDT&E international
www.elsevier.com/locate/ndteint

Eddy currents and hardness testing for evaluation of steel decarburizing

D. Mercier*, J. Lesage, X. Decoopman, D. Chicot

Laboratoire de Mécanique de Lille, LML UMR 8107, U.S.T. Lille, IUT A GMP, BP 179–59653 Villeneuve d'Ascq Cedex, France

Received 3 February 2006; received in revised form 6 April 2006; accepted 10 April 2006
Available online 22 June 2006

Abstract

Usual heat treatments of steels like austenitization are generally conducted in air. In such atmosphere, a part of the atoms of carbon could be removed from the superficial zone of steel. Indeed, those atoms of carbon, combined with oxygen present in atmosphere, can take gaseous form of carbon monoxide due to the great attraction between atoms of carbon and oxygen. This well-known phenomenon is called decarburizing. It can change microstructure to a large extent and, as a result, bring dramatic modifications of mechanical properties of steel, like decrease of fatigue lifetime. To characterize the extent of decarburizing phenomenon, observations by optical microscopy and/or hardness profiles measurements must be performed in a cross section, as it is advised by international standard. Until today, the eddy current technique is used to detect superficial defects. In practice, the control consists to create two groups of available samples or not, from a large sampling. In this study, we propose to estimate the decarburizing extent.

In the present work, different durations of austenitizing at 920 °C temperature before oil quenching (50 °C) were performed on the SAE 92V45 steel in order to obtain various morphologies and different total depths of the decarburized zone. We will show, in the continuation, how eddy currents control is used to assess the level of decarburizing after a Fourier transformation performed on the output signal. This analysis allows us to link the harmonic decomposition of the signal to the duration of the heat treatment and/or to the total decarburizing depth and, consequently, to the mechanical properties.

Keywords: Decarburizing; Eddy current; Carbon diffusion; Microstructure; Hardness

1. Introduction

Apart from iron, carbon is the most important element entering into the composition of steels, since this balance element plays a role on the martensite mechanical properties obtained after heating and quenching. Moreover, manufacturing of mechanical parts requires austenitizing, which cannot be always done in a control atmosphere furnace. This homogenization treatment is able to produce carbon diffusion from the sample core to the external surrounding, facilitated by the oxygen attraction and the high temperature treatment. The phenomenon induces a carbon content variation into the sample and, consequently, negligible carbon content at the surface. The carbon loss at the surface brings out a decrease of the mechanical properties [1]. In spite of its importance from industrial and scientific points of view, very few studies were published in the literature on the subject during the last decades. Nevertheless, we can find some papers on the effect of decarburization on the steel microstructure [2,3], the resistance to corrosion [4] or the impact on fatigue behaviour [5,6]. These demonstrate the necessity for better detection and characterization of the decarburization extent. The International Standard ISO 3887 advises the decarburization control using the two following methods. The first one consists of an optical observation of the microstructure in a cross section of a sample. After etching, the structure differs from the martensitic structure from darker to whiter for ferritic one [7,8]. A disadvantage of the optical control is the limit determination between the decarburized zone and the unaffected steel. In fact, this limit is firstly subjected to analysis errors depending on the cutting, polishing and etching process and, secondly to the operator appreciation. The second method consists in establishing a micro-hardness profile in a cross section of

*Corresponding author. Tel.: +33 320 677326; fax: +33 320 677321.
E-mail address: david.mercier@univ-lille1.fr (D. Mercier).

0963-8695/$ - see front matter © 2006 Elsevier Ltd. All rights reserved.
doi:10.1016/j.ndteint.2006.04.005

the sample after polishing. The two methods are destructive and need considerable preparation. Therefore, they cannot be applied directly during the production process. Nowadays, the eddy current method is based on a large sampling to detect presence of defect. The aim of this technique is to create two groups of samples to separate the good samples and the bad ones. In the present paper, we will examine the possibility to use eddy currents to measure precisely decarburizing depth, since this method is quasi-instantaneous and non-destructive after calibration.

2. Prior eddy current theory

Restivo in 1996 [9] has provided the general way to apply the eddy current theory whereas Yusa et al. [10] applied this theory to the detection of surface defects as well as Zilberstein et al. [11] to control crack initiation and growth during fatigue test. More recently, Uchimoto et al. [12,13] have tried with success to apply eddy current to the study of pearlite proportion in a grey cast iron. For case-carburized steel, Stevens et al. [14] have confirmed, by using TEM and magnetic force macroscopy, that this method is able to determine the microstructure state. In addition, Moorthy et al. [15] and Zergoug et al. [16] have proposed to connect the mechanical micro-hardness modifications induced by carburizing to the magnetic properties variations. These last results have motivated us to apply eddy current methodology to the study of decarburized steels.

Hughes [17] presents in detail the eddy current theory. This theory can be resumed in a short way as follows. By passing an alternative current through a coil, fluctuating electromagnetic fields are created. When the sample is introduced into the coil, the electromagnetic fields induce eddy currents, which change the primary coil impedance. These induced variations depending on the eddy current magnitude, which are as a function of electrical conductivity, magnetic permeability of the sample, test frequency and distance between the coils and the sample. The basic relation for the impedance, according to this phenomenon for a coil of N turns spirally wound, is defined by the well-known Ohm's law

$$\vec{Z} = \frac{\vec{V}}{\vec{i}}, \tag{1}$$

where $\vec{V}$ and $\vec{i}$ are, respectively, the complex vectors of Fresnel associated with the tension and the intensity. $\vec{V}$ and $\vec{i}$ are linked to the complex reluctance (R) of the magnetic circuit and to the magnetic flux ($\vec{\phi}$) by the following relationships:

$$N\vec{i} = R\vec{\phi} \tag{2}$$

and

$$\vec{V} = jN\omega\vec{\phi}, \tag{3}$$

where ω is the current pulsation.

From relation (1), these two last relations allow to determine the complex impedance, which can be written as

$$\vec{Z} = j\frac{\omega N^2}{\vec{R}} = R + jX. \tag{4}$$

The sensor impedance is characterized by resistive component (R) and an inductive term (X). The output signal modified by the impedance variation defined by (4) gives limited information under this form since it is related to a distorted signal. Using fast Fourier transformation (FFT), it is possible to decompose the time function signal into a sum of frequency signals expressed as complex exponential functions. Applied to the output signal, we obtain values of amplitudes and phases for harmonics numbers 3, 5 and 7. We will show that, firstly, harmonics could be validly related to the extent of the decarburized zone and secondly, that eddy current can be an alternative to the classical methods to appreciate the decarburizing depth.

3. Materials and experimental methods

The present investigation is conducted on specimens of SAE 92V45 (54SiCrV6) steel for which chemical composition is given in Table 1. This steel is known for its resistance to grain growth at high temperature because of the presence of vanadium [18]. Then the grain growth, which could occur during austenitizing treatment, is not considered as responsible for the eddy current variations.

Specimens of 20 mm diameter and 100 mm length were cut from bars for which initial metallurgical state was ferrite and pearlite colonies. In order to obtain different situations of carbon depletion, all the samples were maintained at 920 °C during regularly eight different times ranging regularly from 15 to 120 min. This temperature was chosen in order to obtain complete dissolution of the carbides in austenite. After this treatment, samples were oil-quenched to induce martensitic transformation. Samples were referenced from A to H according to the austenitizing time.

The micro-hardness profile was measured with a Knoop indenter on a Leco micro-hardness tester. For

Table 1
Chemical composition in weight percentage

Steel	C	Mn	Si	P	Ni	Cr	Mo	Cu	Sn	Ti	V
54SiCrV6	0.555	0.680	1.565	0.008	0.075	0.510	0.025	0.185	0.013	0.001	0.125

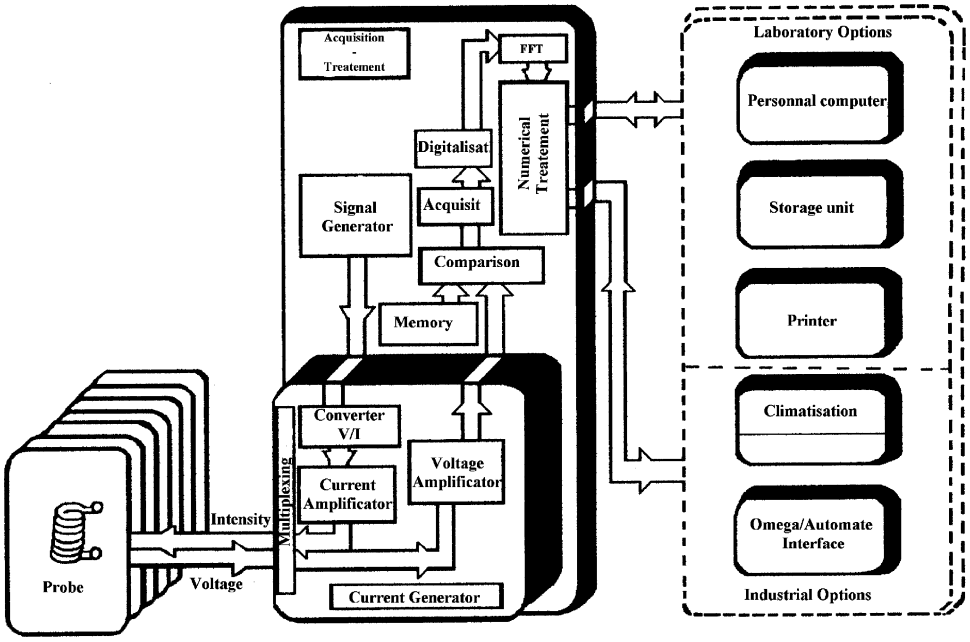

Fig. 1. General synopsis of the experimental apparatus (Alphatest OMEGA 2000).

each modality of austenitizing time, five indentations were performed under a load of 1 N in a cross section perpendicular to the surface, every 20 μm from the surface to a depth of 700 μm. The eddy current equipment used was the Alphatest OMEGA 2000, which allows the acquisition and the decomposition of the output signal. The synopsis of a measurement is presented Fig. 1. The part located at the left shows the probe where the sample is introduced, the middle part is the measuring channel (generator, treatment, etc.) and the last part corresponds to additional options.

The generator provides a sinusoidal current with a frequency (F) ranging from 0.5 to 3 kHz and intensity (I) ranging from 0.1 to 10 A. The output tension is recorded for various couples I_i and F_i and then submitted to the FFT. In a first approximation, harmonics are computed by using a second-degree polynomial fitting for each amplitude and phase parameter according to the austenitizing time. We notice, for each situation of couple (F, I), that harmonics 3, 5 and 7 can be fitted due to the hysteresis symmetry. For these harmonics, the best fit is experimentally found with a couple equal to (50 Hz, 1A).

In the first part, using optical control and micro-hardness profile of the decarburization zone, we compared these two methods by the application of the carbon diffusion theory. In the second part, investigation by eddy currents will be achieved in order to examine the decarburization process with the harmonics amplitudes calculated from FFT. Results obtained by the two methods will be then compared to validate eddy current methodology.

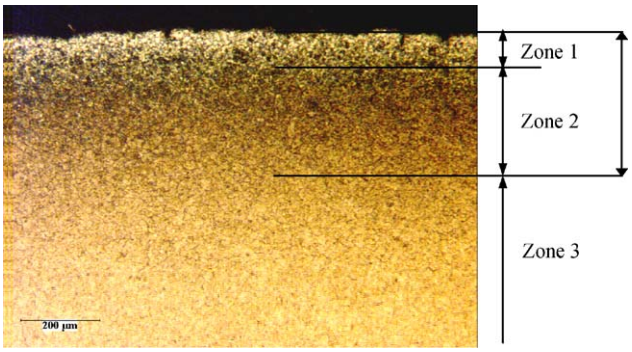

Fig. 2. Optical photography in a cross section of an austenitized sample during 105 min.

4. Results and discussion

4.1. Optical observations

After austenitizing and oil quenching, the samples were sectioned and polished with grade from 6 to 1 μm diamond and etched in Nital 4%. Fig. 2 shows an example of the typical aspect of a decarburized sample.

Three zones of different colours can be noticed in Fig. 2. Close to the surface, the colour is mainly white and corresponds to a structure, entirely composed of very low carbon martensite and/or ferrite, which have the same microstructural aspect. Towards the core, the colour is darker but still exhibits some white spots. These spots correspond to lower carbon martensite associated to spots of ferrite, located where the diffusion of carbon was easier, i.e. at the grain boundaries. In the core, colour is rather

Table 2
Total decarburizing depths estimated by optical measurements

Sample	A	B	C	D	E	F	G	H
Austenitizing time (t in s)	900	1800	2700	3600	4500	5400	6300	7200
Total decarburizing depth (x_{T_0} ±15 in μm)	0	90	95	155	185	245	280	320

homogeneous and associated to a martensite including initial carbon content of steel. The total decarburizing depth is associated to the change of colour between zones 2 and 3. Since it is very gradual, it is difficult to define precisely a boundary between the affected zone near the surface and the core of the material. Table 2 gives an estimation of the total decarburizing depth for all samples in accordance with the corresponding international standard.

As it was expected, the total decarburizing depth increases with the austenitizing time. Since it is governed by the carbon diffusion in austenite, the decarburizing process should satisfy the diffusion equations of Fick. Applied to the problem of carbon diffusion from the surface to the core, the solution of the second Fick's law takes the following form:

$$C(x,t) = C_0 + (C_S - C_0)\left\{1 - \frac{2}{\sqrt{\pi}}\int_0^{x/2\sqrt{Dt}} \exp(-y)\,dy\right\}, \tag{5}$$

where $C(x,t)$ represents the carbon content at a given depth, x, measured from the surface of the sample. The concentration C_S is the carbon content at the surface and C_0, the initial carbon content of the steel. D is the diffusion coefficient of carbon atoms in austenite, which is given by

$$D = D_0 \exp(-Q_A/RT). \tag{6}$$

Here, D_0 represents the diffusivity coefficient. Q_A is the activation energy for the diffusion of carbon in austenite. R is the perfect gas constant equal to 8.314 J/mol K. Nowadays, relations (5) and (6) are well admitted but different values for the diffusivity coefficient can be found in literature. For example, D_0 is equal to 0.1 $cm^2 s^{-1}$ for Roy and Manna [19] whereas it is equal to 0.234 $cm^2 s^{-1}$ for Gamsjager et al. [20]. It should be noticed that the ratio between these two coefficients gives a value higher than 2. Then, to avoid any discussion about choice of such coefficient, we consider the intermediate value of 0.17 $cm^2 s^{-1}$ already used by Lan et al. [21] and Kumar et al. [22] in their studies. Concerning the activation energy, Q_A, all the values available in literature are sufficiently close to considerate a mean value. Indeed, Golovin et al. [23] gives two limits depending on the chromium content in the steel: 135 kJ/mol when no chromium is present and 145 kJ/mol with it. For their part, Gamjager et al. [20] and Agren [24] have used 148 kJ/mol and Lan et al. [21] and Kumar et al. [22], 143.3 kJ/mol. Then, we have retained 145 kJ/mol for Q_A in order to take into account

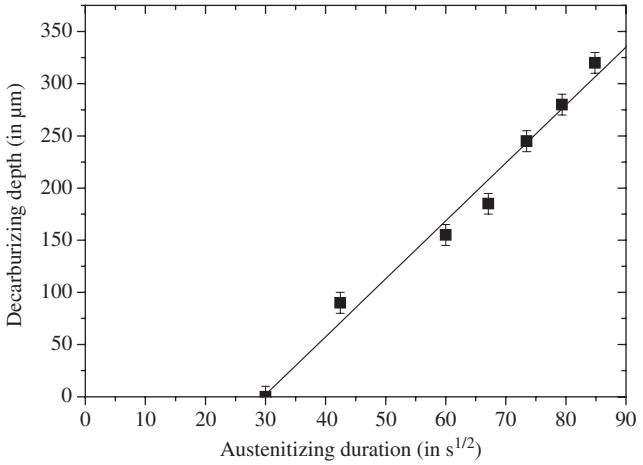

Fig. 3. Decarburizing depth depending on the square root of the austenitizing time.

presence of chromium in the material (see Table 1). By considering values of D_0 (0.17 $cm^2 s^{-1}$) and Q_A (145 kJ/mol), we calculate a diffusion coefficient D equal to 7.6×10^{-8} $cm^2 s^{-1}$ at 920 °C (relation (6)).

Furthermore, total depths of the decarburized zone (x_{T_0}) (Table 2), as it is optically measured, correspond to the limit for which the carbon content, $C(x_{T_0}, t)$, should be equal to the initial concentration of carbon C_0 of the material. In these conditions, according to the second Fick's law, the complementary function error of Gauss should be equal to 0:

$$\left\{1 - \frac{2}{\sqrt{\pi}}\int_0^{x_{T_0}/2\sqrt{Dt}} \exp(-y)\,dy\right\} = \left\{1 - \mathrm{erf}\left(\frac{x_{T_0}}{2\sqrt{Dt}}\right)\right\} = 0. \tag{7}$$

To satisfy this relation, the ratio $x_{T_0}/2\sqrt{Dt}$ should take a constant value higher than 2 according to the calculation of the function error of Gauss and, moreover, it should be independent of the couple (x_{T_0}, t). Then, experimental data collected in Table 2 should satisfy the following relation where the constant ratio, k, should theoretically take a value near 2:

$$\frac{x_{T_0}}{2\sqrt{Dt}} = k \;\text{ or }\; x_{T_0} = s \cdot \sqrt{t} \;\text{ with }\; s = 2 \cdot k \cdot \sqrt{D}. \tag{8}$$

To verify this assumption, we represent in Fig. 3 total decarburizing depths as a function of the square root of the austenitizing time. This figure confirms the linear relation as it was expected but the origin of the straight line is

Fig. 4. Optical photography of the steel surface during 15 min treatment.

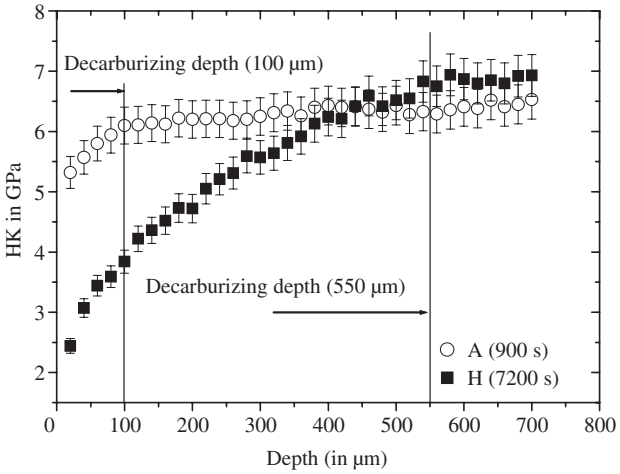

Fig. 5. Micro-hardness evolution for decarburized steels during 15 and 120 min.

different to 0 in contradiction with relation (8). Indeed, the straight line does not intercept the axes at the origin point but at a point corresponding to 15 min of austenitizing time. It is not possible to define if this difference is inherent to the physical phenomenon or to the uncertainty of the optical measurements.

To support this demonstration, Fig. 4 related to sample A confirms that no decarburizing is observable after a heat treatment of 15 min. But that does not involve that the decarburizing phenomenon is not present like we will see it in the following part.

Nevertheless, it is possible by using Eq. (8) to calculate the constant ratio, k, from the slope which is equal to $5.65 \times 10^{-4}\,\mathrm{cm\,s^{-1/2}}$. Consequently, k is equal to 0.98. As a result, $\mathrm{erf}(k) = 0.84$ by applying the function error of Gauss. Therefore, $C(x_{T_0}, t =)0.84\ C_0$ if we assume that C_S is equal to 0 as it was confirmed Fig. 2 by the presence of ferrite at the outer surface. In conclusion, total decarburizing depths, optically measured in each situation of austenitizing, correspond to the same relative carbon content, i.e. 84% of the initial carbons content C_0 of the steel. This means that optical measurements lead, in all the cases, to an underestimation of the total decarburizing depth.

4.2. Micro-hardness measurements

Relation between micro-hardness and microstructure of materials is well known [24–26]. For example, hardness of martensite is a function of the carbon content, from 200 HV for 0.2%C to 1000 HV for 1.0%C. Consequently, decrease of carbon content in the material will give martensite of lower hardness after quenching. Fig. 5 shows two profiles of micro-hardness obtained for samples austenitized during 900 s (A) and 7200 s (H). For intermediate austenitizing times, all curves are situated between these two limits.

In all cases, decrease in hardness is observable from the surface to the material core where it remains constant. This remark is not in accordance with Fig. 4, where low carbon structures are not observed. In this case, the limit between the two zones is easier to determine. For example, it is observed in Fig. 5 that total decarburizing depths are estimated to 100 µm for sample (A) and 550 µm for sample (H). Table 3 collects the total decarburizing depths obtained for each situation of treatment.

From Table 3, data of decarburizing depth are presented as a function of the square root of the austenitizing time in Fig. 6. Data obtained from optical observations are also represented to allow a comparison.

Like the optical observations, the line associated to hardness measurements does not intercept the x-axis at the origin but at a point corresponding to an austenitizing time near 300 s. This seems to indicate that an incubation time is necessary for decarburizing initiation. Such an incubation time is similar to the time necessary for the onset of a nitride combination layer during nitriding [27].

The slope of the straight line is found equal to $7.93\,10^{-4}\,\mathrm{cm\,s^{-1/2}}$, associated to a constant ratio, k, near 1.44 corresponding to $\mathrm{erf}(k) = 0.96$ (i.e. 96% of the initial carbon constant compared to the 84% obtained from optical observations). To conclude, micro-hardness measurements are more accurate than optical measurements for the determination of decarburizing depth and even if this result was expected, we demonstrate that mechanical parameters like hardness are not always in accordance with the micro-structural observations. Thus, micro-hardness measures are able to give precise estimations, but they are destructive. In the continuation, we will present an alternative method that could be used for non-destructive characterization of the decarburizing zone, in particular to appreciate the decarburizing depth.

4.3. Eddy current study

By applying the eddy current theory to the samples, we have obtained a complete description of the output tension

Table 3
Total decarburizing depths estimated from hardness measurements

Sample	A	B	C	D	E	F	G	H
Austenitizing time (t in s)	900	1800	2700	3600	4500	5400	6300	7200
Decarburizing depth (x_{T_H} ±20 in μm)	100	180	260	350	330	410	490	550

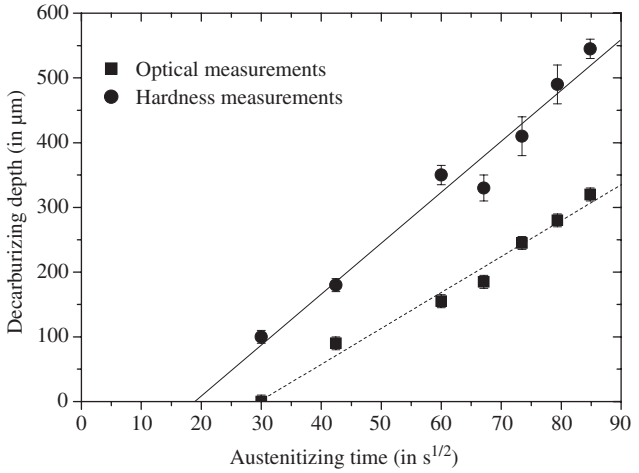

Fig. 6. Decarburizing depth depending on the square root of the austenitizing time.

signal (fundamental and harmonics). As mentioned above, only harmonics 3, 5 and 7 will be used to characterize the decarburizing depth. The values of the vector modulus, the imaginary and the real parts are presented in Table 4.

The vector moduli of harmonics are firstly plotted versus the austenitizing time (Fig. 7). In linear coordinates, Fig. 7a shows that the modulus increases rapidly in function of the austenitizing time and allows to separate bad data points, i.e. corresponding to sample (C).

In logarithmic coordinates for the modulus, the relation becomes linear (Fig. 7b). Under this form, the representation allows to better discriminate additional bad data points (i.e. sample (B)). The deviation of the modulus is interpreted as a technical problem of the eddy current measurement or non-homogeneity of the microstructure of the sample. Whatever is the origin of the problem, optical observations or/and micro-hardness measurements do not permit to detect such defect. From a mathematical point of view, it is possible to represent the modulus as a function of the time, t (in s), and the order number of the harmonic, n, by the following relationship:

$$\Pi = \Pi_0 \cdot \frac{\exp[6.25 \times 10^{-4}\, t]}{n^{7/4}}, \tag{9}$$

where Π_0 is a constant equal to 69.

This relation, represented in Fig. 7 with black lines, gives a good correlation of the data points. Then, it is possible to define, by using relation (8), a criterion of decarburizing, as a critical value for Π, corresponding to a critical value or an acceptable decarburizing depth from industrial point of view. We will study the possibility to obtain more information by using separately the imaginary part and the real part of the three harmonics. Fig. 8 shows these two parts of the harmonics in function of the austenitizing time.

The imaginary part of the harmonics, which corresponds to the signal phase, is often used to verify the homogeneity of the experimental data. The representation of these data in Fig. 8a, confirms that the values, associated to sample B and in a more obvious way to sample C, are not in accordance with the results obtained for the other samples, as well as the result deduced from the analysis of the modulus. In a second time, real part of the harmonics can be used to characterize the extent of decarburizing. Indeed, as it is observed in Fig. 8b, the amplitude of the signal increases with the austenitizing time and consequently with the extent of decarburizing. By replacing austenitizing time by the corresponding total decarburizing depth, collected in Table 3, allows obtaining a relation between the real part of the harmonics and the total decarburizing depth (Fig. 9).

It is noticed that the variations of the real part of the harmonics can be related to the total decarburizing depth. For the present study, only one of the harmonics could have been used to represent the decarburizing since the three harmonics are strongly related. An exponential relation having the general form applied to describe variation of the modulus (relation (9)) can represent their evolution as a function of the total decarburizing depth

$$R = \pm R_0 \cdot \frac{\exp[0.011 x_{T_H}]}{n^{3/2}}, \tag{10}$$

where R is the real part of the harmonic (i), R_0 is a constant equal to 9.73 and x_{T_H} the total decarburizing depth. Sign (−) is used for harmonics 3 and 7 and sign (+) for harmonic 5. A criterion could be defined as a critical value for the decarburizing depth, $x_{T_{\text{critical}}}$, by rewriting relation (10)

$$x_{T_{\text{critical}}} = \frac{1}{0.011} \cdot \ln\left[\pm\left(\frac{R}{R_0}\right) \cdot n^{3/2}\right]. \tag{11}$$

In order to consolidate such criterion, we study now the relation between real part of the harmonics and the Knoop hardness measured at a given depth. Using bi-logarithmic coordinates, Fig. 10 shows a linear correlation between micro-hardness measured at 20 μm from the surface and the real part of the harmonics with a correlation coefficient around 0.95 for each harmonic.

Furthermore, it seems to be interesting to study the harmonic behaviour according to its number [9]. This

Table 4
Real and imaginary parts from signal decomposition and the values of corresponding vector modulus

Sample		A	B	C	D	E	F	G	H
Time of austenitizing (min)		15	30	45	60	75	90	105	120
Imaginary part of the harmonic (in rad modulo 2π)	3	−16	−70	−646	−52	−46	−164	−222	−672
	5	−8	52	464	−14	−42	−26	−18	138
	7	−4	−32	−354	6	36	64	66	22
Real part of the harmonic (dB)	3	4	−24	8	−92	−130	−240	−304	−540
	5	−2	−4	12	28	52	150	192	422
	7	2	−2	−40	−18	−16	−68	−94	−254
Vector modulus = Π	3	16	74	646	106	138	291	376	862
	5	8	52	24	31	67	152	203	444
	7	4	32	356	19	39	93	115	255

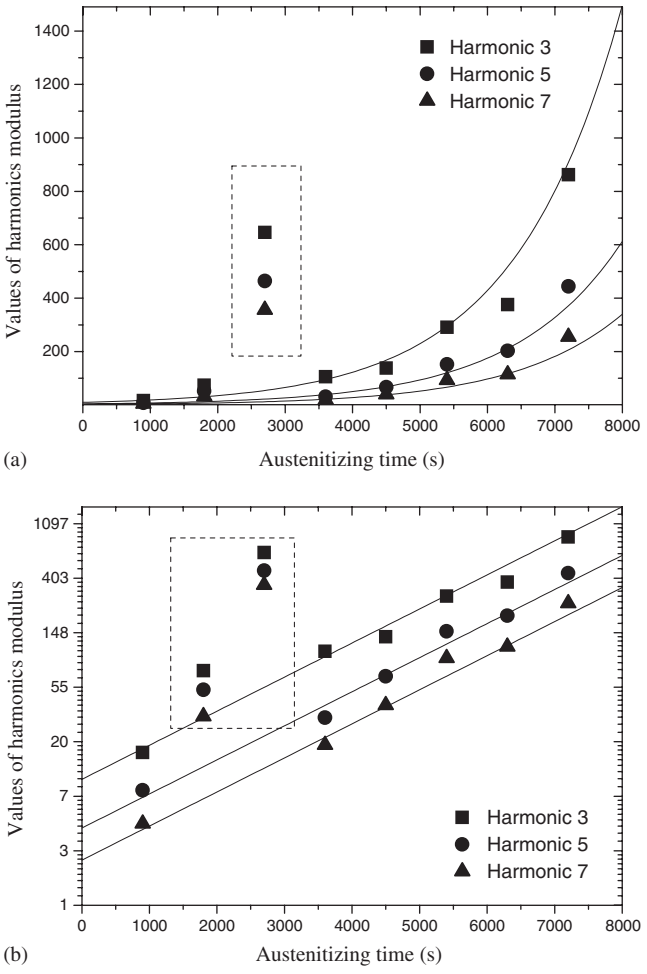

Fig. 7. Vector modulus of the 3, 5 and 7 harmonics as a function of the austenitizing time.

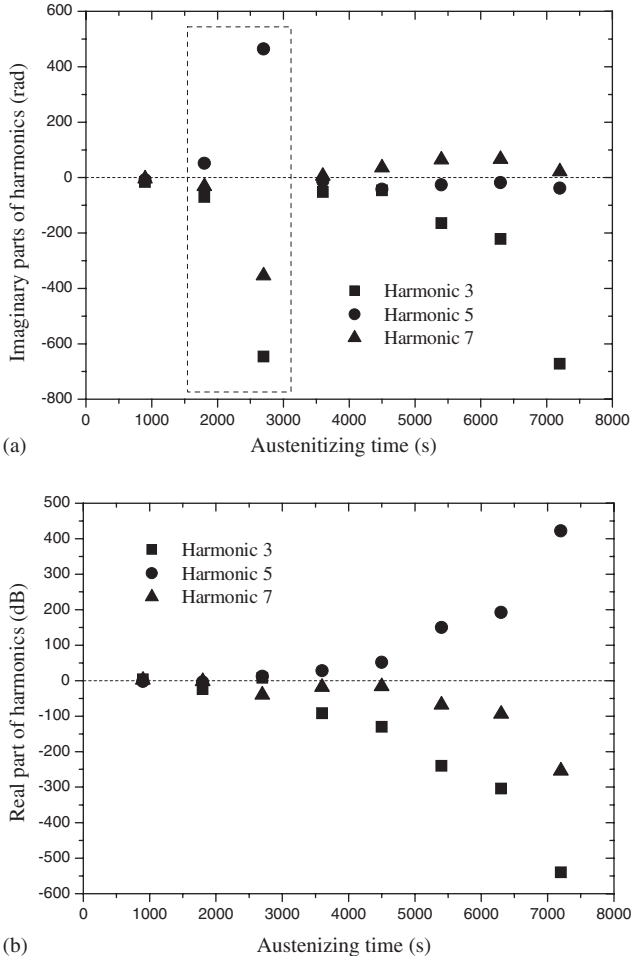

Fig. 8. Imaginary (a) and real parts (b) of the 3, 5 and 7 harmonics depending on the austenitizing time.

assumption is studied by plotting the coefficient of correlation, calculated on the straight line $\ln|\mathrm{Re}| = f(\ln HK)$ relating to several depths, (x_{HK}), corresponding to the location of the hardness measurement. Fig. 11 represents the variation of the correlation coefficient according to the depth (x_{HK}).

This figure clearly shows that the correlation coefficient is better with a higher harmonic number when the corresponding depth (x_{HK}) is higher. Therefore, the choice of the harmonic depends on the frequency of the fundamental, which is an important parameter since it could lead to a pre-magnetization for the higher harmonic.

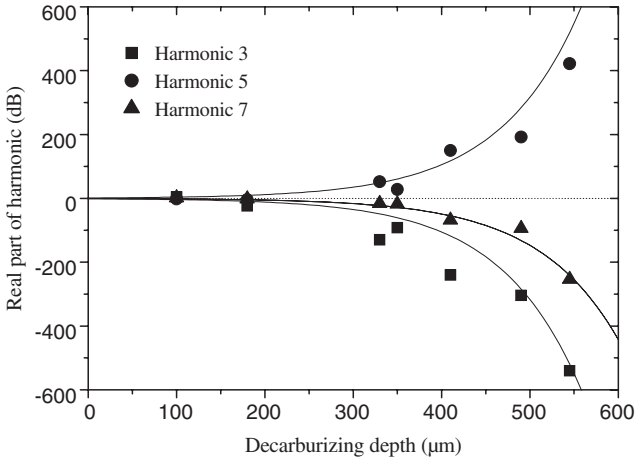

Fig. 9. Real part of the harmonics relating to the decarburizing depth (hardness measurement).

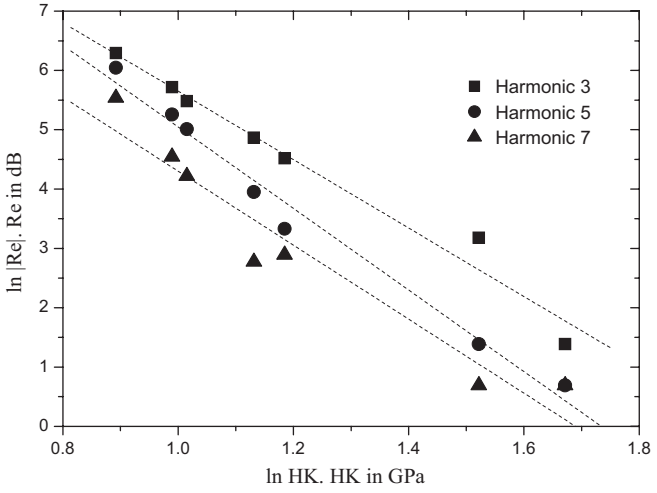

Fig. 10. Correlation between surface hardness and the harmonics real part.

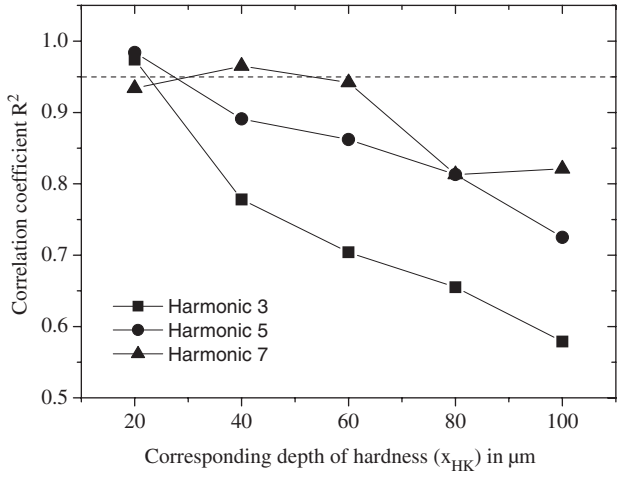

Fig. 11. Correlation coefficient according to the corresponding depth of hardness (x_{HK}).

And, as a consequence, it depends also on the depth where the characterization should be done.

5. Conclusions

In the present paper, we have shown that optical measurements underestimate the decarburized depth of heat-treated steel as regards to the micro-hardness. Indeed, micro-hardness measurements are more efficient and they must be used to calibrate the eddy current measurements despite the micrographic analysis. It was shown that the eddy current technique is very sensitive and well related to surface modifications associated to the decarburizing phenomenon. In order to be used as a systematic means for industrial control, it needs only to be performed on reference samples of known hardness or carbon content. We propose also a criterion of decarburizing, which could be used to estimate the total decarburizing depth. But, there is still some work to do, anyway, to be able to assess the hardness variations due to carbon content modifications by using over the entire decarburized zone. Moreover, the harmonics analysis, in particular calculation of parameters Π and R, should take into account the composition of the studied steel.

References

[1] Wei S, Jinhua Z, Liujie X, Rui L. Effects of carbon on microstructures and properties of high vanadium high-speed steel. Mater Des 2005;17:58.
[2] Brown AF, Hayes DJ. Observations on the decarburization and graphitisation of steels by sodium. J Nucl Mater 1968;127:187.
[3] Standaert C, Eloot K, De Paepe A, Wokowski P. Decarburization of interlocked and laser welded stator and rotor cores. J Magn Magn Mater 1996;160:139.
[4] Rademakers PLF, Kolster BH. Corrosion of various ferritic steels in an isothermal sodium loop system. J Nucl Mater 1981;97:309.
[5] Waterhouse RB, Taylor DE. The effect of heat treatment and decarburization on the fatigue behaviour of a 0.7% carbon steel. Proc Inst Mech Eng Wear 1972;19:364.
[6] Granottier C. Contribution à l'étude de la tenue en fatigue des ressorts formés à chaud : influence cumulée des parametres de surface. Thèse de Doctorat 1982. Ecole Centrale de Lyon. N° d'ordre 82-04.
[7] Vöhringer O, Macherauch E. HTM 1977;32:153.
[8] Kurdjumov GV. Martensite crystal lattice, mechanism of austenite–martensite transformation and behavior of carbon atoms in martensite. Metall Trans 1976;7A:999.
[9] Restivo MT. A case study of induced eddy currents. Sensors Actuators A: Phys 1996;51:203.
[10] Yusa N, Cheng W, Uchimoto T, Miya K. Profile reconstruction of simulated natural cracks from eddy currents signals. NDT & E Int 2002;35:8.
[11] Zilberstein V, Walrath K, Grundy D, Schlicker D, Goldfine N, Abramovici N, et al. MWM eddy currents array for crack initiation and growth monitoring. Int J Fatigue 2003;25:1147.
[12] Uchimoto T, Takagi T, Konoplyuk S, Abe T, Huang H, Kurosawa M. Eddy current evaluation of cast irons for material characterization. J Magn Magn Mater 2003;258:259–493.
[13] Konoplyuk S, Abe T, Uchimoto T, Takagi T, Kurosawa M. Characterization of ductile cast iron by eddy current method. NDT & E Int 2005;38(8):623–6.

[14] Stevens KJ, Parbhu A, Soltis J. Magnetic force microscopy and cross-sectionnal transmission electron microscopy of carburised surface. Curr Appl Phys 2004;4:304.
[15] Moorthy V, Shaw BA, Evans JT. Evaluation of tempering induced changes in the hardness profile of case-carburised EN36 steel using magnetic Berkhausen noise analysis. NDT & E Int 2003;36:43.
[16] Zergoug M, Lebaili S, Boudjellal H, Benchaala A. Relation between mechanical microhardness and impedance variation in eddy current testing. NDT & E Int 2004;37:65.
[17] Hughes DE. The cause of evident magnetism in iron, steel, and other magnetic metals. J Franklin Inst 1883;116(2):128–50.
[18] Bensimon R. Les Aciers. PYC Editions 1971;2:68.
[19] Roy A, Manna I. Mathematical modelling of localized melting around graphite nodules during laser surface hardening of austempered ductile iron. Opt Lasers Eng 2000;34:369.
[20] Gamsjager E, Antretter T, Schmaranzer C, Preis W, Chimani CM, Simha NK, et al. Diffusion phase transformation and deformation in steels. Comput Mater Sci 2002;25:92.
[21] Lan YJ, Li DZ, Li YY. Modelling austenite decomposition into ferrite at different cooling rate in low-carbon steel with cellular automaton method. Acta Mater 2004;52:721.
[22] Kumar M, Sasikumar R, Kesavan Nair R. Acta Mater 1998;46:6291.
[23] Golovin IS, Nilsson JO, Serhantova GV, Golovin SA. Anelastic effects connected with isothermal martensite transformations in 24Ni4Mo austenitic and 12Cr9Ni4Mo maraging steels. J Alloys Compd 2000;310:411.
[24] Agren J. A simplified treatment of the transition from diffusion controlled to diffusionless growth. Acta Metall 1989;37:181.
[25] Erdogan M, Tekeli S. The effect of martensite particle size on tensile fracture of surface carburised AISI 8620 steel with dual phase core structure. Mater Des 2002;23:597.
[26] Murry G. Transformations dans les aciers. Techniques de l'Ingénieur, M1-115.
[27] Rozendaal HCF, Mittemeijer EJ, Coljin PG, Van der Schaaf PJ. The conversion cementite $\rightarrow \varepsilon$-nitride during the nitriding of FeC-alloys. Scipta Metall 1980;14(11):1189–92.